Mechanisms underlying temperature extremes in Iberia: a Lagrangian perspective

Tellus SERIES A DYNAMIC METEOROLOGY AND OCEANOGRAPHY
PUBLISHED BY THE INTERNATIONAL METEOROLOGICAL INSTITUTE IN STOCKHOLM

Mechanisms underlying temperature extremes in Iberia: a Lagrangian perspective

By JOÃO A. SANTOS[1,2]*, STEPHAN PFAHL[3], JOAQUIM G. PINTO[4,5] and HEINI WERNLI[3], [1]*Physics Department, School of Sciences and Technology, Universidade de Trás-os-Montes e Alto Douro, Vila Real, Portugal*; [2]*Centre for the Research and Technology of Agro-Environmental and Biological Sciences, CITAB, Universidade de Trás-os-Montes e Alto Douro, UTAD, Vila Real, Portugal*; [3]*Institute for Atmospheric and Climate Science, ETH Zurich, Zurich, Switzerland*; [4]*Department of Meteorology, University of Reading, Reading, United Kingdom*; [5]*Institute for Geophysics and Meteorology, University of Cologne, Cologne, Germany*

(Manuscript received 16 September 2014; in final form 4 March 2015)

ABSTRACT

The mechanisms underlying the occurrence of temperature extremes in Iberia are analysed considering a Lagrangian perspective of the atmospheric flow, using 6-hourly ERA-Interim reanalysis data for the years 1979–2012. Daily 2-m minimum temperatures below the 1st percentile and 2-m maximum temperatures above the 99th percentile at each grid point over Iberia are selected separately for winter and summer. Four categories of extremes are analysed using 10-d backward trajectories initialized at the extreme temperature grid points close to the surface: winter cold (WCE) and warm extremes (WWE), and summer cold (SCE) and warm extremes (SWE). Air masses leading to temperature extremes are first transported from the North Atlantic towards Europe for all categories. While there is a clear relation to large-scale circulation patterns in winter, the Iberian thermal low is important in summer. Along the trajectories, air mass characteristics are significantly modified through adiabatic warming (air parcel descent), upper-air radiative cooling and near-surface warming (surface heat fluxes and radiation). High residence times over continental areas, such as over northern-central Europe for WCE and, to a lesser extent, over Iberia for SWE, significantly enhance these air mass modifications. Near-surface diabatic warming is particularly striking for SWE. WCE and SWE are responsible for the most extreme conditions in a given year. For WWE and SCE, strong temperature advection associated with important meridional air mass transports are the main driving mechanisms, accompanied by comparatively minor changes in the air mass properties. These results permit a better understanding of mechanisms leading to temperature extremes in Iberia.

Keywords: temperature extremes, cold episodes, warm episodes, Lagrangian trajectories, large-scale circulation, surface fluxes, Iberian Peninsula, ERA-Interim

1. Introduction

Temperature extremes, like heat waves and cold spells, have a strong impact on the environment and society (Alexander et al., 2006; Hanson et al., 2007; Seneviratne et al., 2012), and their occurrence in Europe is commonly associated with anomalous large-scale atmospheric conditions (e.g. Santos and Corte-Real, 2006; Cony et al., 2008; Efthymiadis et al., 2011; Andrade et al., 2012; Moore and Renfrew, 2012; Pfahl and Wernli, 2012). The occurrence of temperature extremes has been reported to increase in recent decades (e.g. Tank and Können, 2003; Seneviratne et al., 2014), a trend that is also projected for future decades (IPCC, 2013; Kharin et al., 2013), also for Europe (Cattiaux et al., 2012; Frías et al., 2012). In particular, the occurrence of heat waves is expected to increase in terms of their frequency, intensity and duration (Fischer and Schär, 2010; Seneviratne et al., 2012). Owing to the strong impacts of weather extremes on many socio-economic sectors worldwide (Cooney, 2012; Field et al., 2012; Murray and Ebi, 2012; Orlowsky and Seneviratne, 2012), studying their underlying processes is of foremost relevance.

The Iberian Peninsula (IP) is an area frequently affected by such extremes. Moreover, an increase in frequency and

*Corresponding author.
email: jsantos@utad.pt

Citation: Tellus A 2015, **67**, 26032, http://dx.doi.org/10.3402/tellusa.v67.26032

intensity is projected for future decades (Ramos et al., 2011; Andrade et al., 2014). The occurrence of temperature extremes in the IP tends to be driven by large-scale circulation anomalies, particularity in the winter half of the year and over the western half of the peninsula, when and where a strong linkage exists to the North Atlantic Oscillation (NAO) and East Atlantic (EA) pattern (e.g. Ulbrich et al., 1999; Trigo et al., 2002, 2004; García-Herrera et al., 2007; Santos et al., 2007). The location of the North Atlantic jet stream, with three preferred regimes (northern, central and southern regimes after Woollings et al., 2010), has been shown to strongly impact temperature extremes in Europe, also with significant signatures in Iberia (Mahlstein et al., 2012). For instance, the central regime is mostly unfavourable for temperature extremes in Iberia, while they occur primarily in the northern and southern regimes (e.g. winters of 2010 and 2012; cf. Santos et al., 2013b). Based on the aforementioned studies, temperature advection, radiation and surface fluxes are all expected to play a key role for the occurrence of temperature extremes over the IP. However, their relative weight has not yet been determined for the different types of extreme (cold/warm) and in the different seasons (winter/summer).

The Lagrangian perspective on the formation of temperature extremes permits a more quantitative understanding of the associated physical mechanisms (Bieli et al., 2014). Calculating backward trajectories of surface air masses associated with extreme temperature episodes (Lagrangian approach) enables not only to identify their origin, but also the physical mechanisms that occur along their pathway and the modification of their thermodynamic properties (Wernli and Davies, 1997). The temperature of a given air parcel can change through: (1) adiabatic cooling/warming, related to ascending/descending motion; and (2) diabatic fluxes that comprise latent and sensible heat fluxes, shortwave/solar radiation and long-wave/thermal radiation (Holton, 2004). The temperature at a given site (Eulerian approach) can also change through (horizontal and vertical) temperature advection (Holton, 2004).

The primary aim of this study is to identify the main physical mechanisms leading to temperature extremes affecting the IP. This provides not only a better understanding of the underlying physical processes, but also helps assess the skill of climate models in replicating the natural processes driving weather extremes, either in weather forecasting or decadal/long-term climate projections (Solomon et al., 2011). The main focus of the analysis is the continental area of the IP (Fig. 1). However, the strong contrast between the North Atlantic-facing (northern and western) and the Mediterranean-facing (eastern and southern) regions of the IP, which is significantly enhanced by several mountain ranges and by the latitude range from 35 to 44°N (between subtropical highs and mid-latitude lows), leads to a large diversity of climatic conditions across the peninsula (Tullot, 2000; Santos et al., 2013a). Therefore, the regional climatic specificities of the IP also justify the study of subsectors, as the mechanisms underlying temperature extremes might be different between, for example, eastern and western Iberia. The structure of the paper is as follows: data and methods are described in Section 2, results are presented in Section 3 and a summary of the main conclusions and their discussion are provided in Section 4.

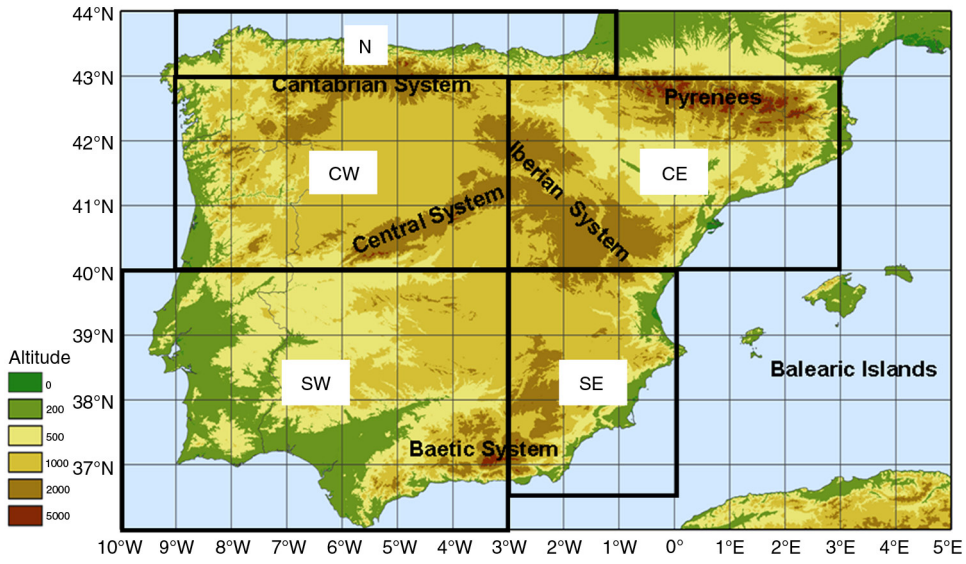

Fig. 1. Orographic map of the Iberian Peninsula (altitude in m), along with the main mountain ranges, and the subsectors for regional assessments (see also Table 1).

2. Data and methods

Following Bieli et al. (2014), the Lagrangian analysis tool LAGRANTO (Wernli and Davies, 1997) is applied to calculate 10-d backward trajectories of surface air masses associated with temperature extremes in the IP. With this purpose, all atmospheric variables are retrieved every 6 hours from the ERA-Interim reanalysis dataset of the European Centre for Medium-Range Weather Forecasts (Dee et al., 2011), for the period from 1979 to 2012 (34 yr) on a 1.0° latitude × 1.0° longitude grid (ca. 80–100 km grid spacing). Temperature extremes are considered at 91 grid points in the Iberian sector, which we define as the region from 37 to 43°N and 9°W to 3°E, that is, with seven grid points in the meridional and 13 in the zonal direction. Six-hourly cold/warm extremes are defined at each grid point for 6-hourly minimum/maximum 2-m air temperature (T2MIN/T2MAX) below/above the 1st/99th percentile of the full empirical distribution at that grid point. The use of these percentile-based indices is widespread in climate research and particularly suitable for isolating extremes over regions with very heterogeneous climates (Zhang et al., 2011), such as the IP (Tullot, 2000; AEMET/IMP, 2011). Back-trajectories are then computed in order to identify the origin of air masses associated with the extreme events. They are started at the time of the extreme episode onset, and air parcels are traced backwards in time. Thus, the trajectory start time corresponds to the onset of the extreme event, while their ending corresponds to their earliest stage (several days before the onset of the event).

Owing to strong seasonality, cold and warm extremes are considered separately for winter (DJF) and summer (JJA). Hence, the number of extremes at each grid point is 1% of 34 yr × 90/92 d × 4 times a day, that is, 122/125 extremes of each type for winter/summer. Thus, for the whole sector (91 grid points), there is a sample of 11 102 local cold/warm extremes for winter and 11 375 for summer. Trajectories were started at three pressure levels (10-, 30- and 50-hPa above the surface) at the grid points with an identified temperature extreme, which accounts for vertical variations in the boundary layer (Bieli et al., 2014). This approach inherently takes into account vertical mixing in the boundary layer at the location of the extreme event, which is not explicitly resolved in the 6-hourly ERA-Interim data. Because extremes typically occur simultaneously at multiple nearby locations and sometimes during several 6-hourly periods of the same day, the total number of non-simultaneous daily events is effectively much lower than the number of tracked trajectories: 498 for winter cold extremes (WCE), 562 for winter warm extremes (WWE), 490 for summer cold extremes (SCE) and 983 for summer warm extremes (SWE). Although some events are represented by a relatively large number of trajectories (large-scale cold/warm events that last for several time steps), the total number of independent events per season is high enough such that single days do not dominate the overall results. While the winter extremes (WCE and WWC) have a comparable number of distinct days, the number of distinct daily SWE episodes is almost three times as large as for SCE. Given the seasonality, WCE and SWE are typically responsible for the most extreme conditions in a given year.

Following Bieli et al. (2014), several variables are tracked (using linear interpolation in space and time) and analysed over the 10-d period preceding the extreme events in order to characterize the trajectories. Latitude, longitude and pressure jointly determine the location of the air mass at a given instant. For the thermodynamic characterization of the air parcel, temperature, potential temperature (theta), specific humidity and relative humidity are tracked. Furthermore, the following surface/near-surface variables beneath the trajectory are also considered: 2-m minimum (T2MIN) and maximum (T2MAX) temperatures, and anomaly indices (following Bieli et al., 2014) of surface sensible heat flux (SSHF), surface latent heat flux (SLHF), surface thermal radiation (STR) and surface solar radiation (SSR). In the present study, positive SLHF, SSHF and STR are directed from the surface to the atmosphere, while positive SSR is directed towards the surface. Daily anomalies of these surface fluxes with respect to the local climatology (dimensionless anomalies) are calculated by subtracting the local mean value of each 6-hourly time step and dividing through the sum of the 6-hourly standard deviations (cf. Bieli et al., 2014). Positive anomalies indicate more intense fluxes compared to climatology (SLHF, SSHF and STR) or enhanced solar radiation (SSR). Due to the construction of the anomaly indices, values between 0.5 and 1 already represent relatively strong anomalies compared to the climatology. The representation of surface fluxes in reanalysis data still has important limitations (Decker et al., 2012) and thus the results concerning the fluxes must be interpreted with care.

In order to assess regional heterogeneities in the temperature extremes, a sectorial analysis is also carried out for five subsectors (Fig. 1 and Table 1). A higher number of subsectors could better capture regional climate heterogeneities, but the outcomes would become less robust due to the small sample sizes.

3. Results

3.1. Winter cold extremes

The WCE episodes affecting the IP are fundamentally associated with northeasterly transport of very cold and dry air masses from central-northern Europe, reaching the IP mostly through the western-central Pyrenees and the northern (Cantabrian) coast (Fig. 2a–c). Their paths exhibit strong

Table 1. List of the Iberian subsectors, also defined by their latitude and longitude ranges

Subsector	Latitude	Longitude
N – Northern Iberia	43.0–44.0°N	1.0–9.0°W
CW – Central-western Iberia	40.0–43.0°N	3.0–9.0°W
SW – South-western Iberia	36.0–40.0°N	3.0–10.0°W
CE – Central-eastern Iberia	40.0–43.0°N	3.0°W–3.0°E
SE – South-eastern Iberia	36.0–40.0°N	3.0°W–0.0°

similarity, which is highlighted by the high densities observed over the continent up to 5 d before the onset of the episodes in the IP. Many trajectories also reveal earlier northerly/northwesterly paths over the high-latitude North Atlantic and northern Europe (Fig. 2a). Streamlines of the wind at 850 hPa are used to analyse the air flow and the representative synoptic-scale features in the lower-troposphere. The composite streamlines (averaged over all WCE episodes) highlight the presence of a fast-growing and strong anticyclonic ridge over the eastern North Atlantic, indicating an omega-like blocking to the west of the British Isles (Fig. 2a–c). A closed low-pressure system develops over the central Mediterranean, reinforcing the northerly flow towards Iberia. North Atlantic atmospheric blocking has been related to the occurrence of European winter cold air outbreaks (Walsh et al., 2001; Sillmann et al., 2011). Despite being composites, the streamlines suggest a frequent occurrence of anticyclonic upper-level wave-breaking over Europe during these episodes, which is also in agreement with the upstream blocking occurrence (Woollings et al., 2008). These synoptic features are consistent with the prevalent northeasterly paths of the parcel trajectories, though streamlines are not coincident with parcel trajectories in a non-stationary flow. These paths are also reflected in the corresponding latitude–longitude plot of the median trajectory (Fig. 2d), also for the subsectors of the IP (cf. Fig. 1 and Table 1). The air flows towards northern Europe at about 60°N and then sharply bends southwestward, with a total zonal (meridional) displacement over Europe of ca. 15° (20°), hinting at the highly advective nature of the WCE episodes. While the translation speed is quite low during the first half of the 10-d period, a rapid displacement is noteworthy in the last 3 d.

Despite some differences between sectors, there is a clear resemblance in the shape of their median paths. The more eastern median path for CE compared to SW can be largely explained by the geographical location of these two sectors, as trajectories for the former often pass the Pyrenees, whereas trajectories for the latter are mostly confined to the northern coast of the IP and western edge of the Pyrenees (not shown) and are thus moderated by a short period over the Bay of Biscay before entering the IP. As the continent is relatively cold compared to the ocean in winter, trajectories over the continent are warmed less by surface fluxes than over the ocean. Therefore, these continental northeasterly paths bring anomalously cold air masses into the IP.

In spite of inter-episode variability, a coherent descent of the air masses is observed along the trajectories (about 200 hPa in 10 d, Fig. 2e), resulting in a strong adiabatic warming of ~ 20°C for the dry lapse rate, reinforcing the leading role played by horizontal advection in triggering these cold extremes. In addition, there is some diabatic cooling (steady decrease in potential temperature) not entirely offset by the abrupt but short-duration warming near the surface (Fig. 2f). For the WCE episodes, when the air parcels reach near-ground levels over the IP, 90% of the trajectories are associated with 2-m minimum temperatures approximately ranging from -10°C to 5°C (Fig. 2g), attesting the coldness of these episodes for Iberian standards. The median increase in the 2-m minimum temperature at the air parcel position over the 10-d period, from -10°C (at high latitudes) to nearly 0°C (in the IP), is coherent with the cold advection driven by the northeasterly flow. Note that Fig. 2f shows a strong warming of the considered air parcels due to adiabatic compression, whereas the associated 2-m temperature reveals a much weaker warming.

As the trajectories enter the boundary layer, they get in contact with the warmer surface and are affected by strong heat and radiation fluxes. This is supported by the highly positive anomalies of SSHF and STR (enhanced heat fluxes from the surface to the atmosphere) during the last 3 d (Fig. 2h). These strong STR anomalies are associated with cold nights with clear sky and strong radiative cooling that typically occur for WCE. The gradual diabatic cooling of the air masses (through net radiative deficits at high latitudes) is also manifested in negative anomalies of SSR during the first 5 d (Fig. 2h). The median air parcel temperature increases by about 20°C in 10 d (Fig. 2f), which is in agreement with descent and adiabatic warming found for other European regions (Bieli et al., 2014). The final temperatures are much higher for SW (3°C) than for CE (-4°C) (Fig. 2f), which can be explained by the stronger maritime influence in the SW compared to CE. Note the much weaker diabatic cooling in SW than in CE (Fig. 2f). In effect, most SW trajectories only enter the IP after travelling a short period over the North Atlantic, and typically have more westerly pathways (Fig. 2d), even though they experience an additional diabatic cooling (Fig. 2f) when travelling over inner Iberia. A similar near-surface diabatic cooling is also observed for CW, but much less pronounced. The continental path of the trajectories for WCE episodes is also manifested by very low specific humidity values (< 3 g kg^{-1}), even at near-surface levels (Fig. 6a). Furthermore, relative humidity undergoes a slight increase and presents relatively high values, despite some decrease at the latest stage of the trajectory due to near-surface

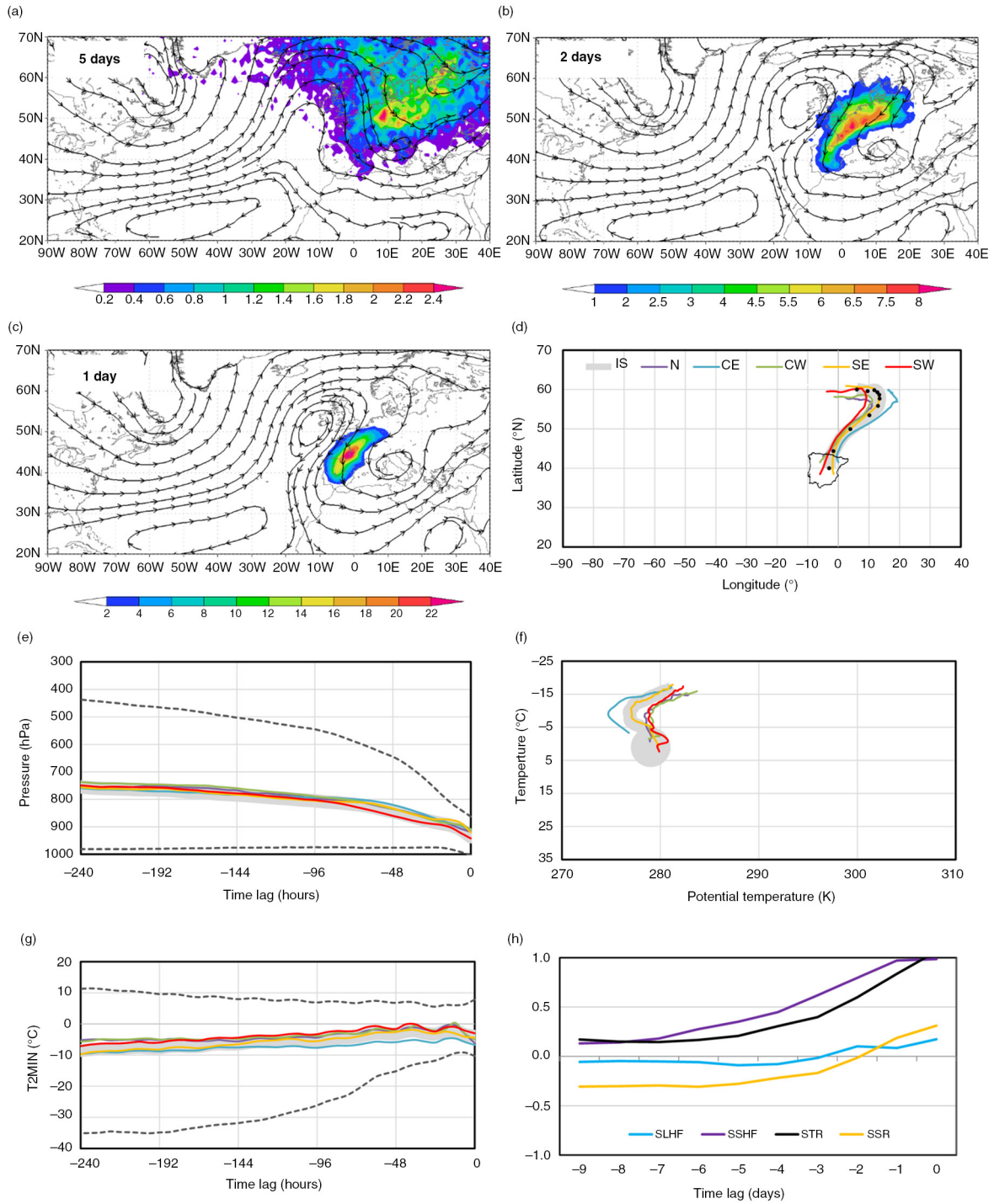

Fig. 2. Wintertime (DJF) extremely cold episodes, WCE, for the period of 1979–2012 (34 yr). (a–c): Trajectory density patterns (in number of trajectories per 1000 km^2, note the different scales), along with the respective composites of 850 hPa streamlines, for the indicated time lags (5, 2 and 1 d before the episode onset). (d–g): Median evolution of the outlined variables along the trajectories for the whole IS (Iberian sector, thick grey line) and for each subsector separately (cf. Fig. 1 and Table 1). The corresponding 5th/95th percentiles for the IS are also displayed in the chronograms (dashed lines in e and g). Black circles in (d) indicate days (from 10 days before onset to onset), while the grey circle in (f) indicates the trajectory at the episode onset. (h): Medians of SLHF, SSHF, STR and SSR anomalies (dimensionless) along the air parcel trajectories (positive SLHF, SSHF and STR directed from surface to atmosphere, positive SSR directed towards the surface).

warming. In general, the increase in specific humidity is largely balanced by the air parcel warming, resulting in only slight changes in relative humidity.

3.2. Winter warm extremes

The WWE episodes affecting the IP can be mainly attributed to westerly/southwesterly flow regimes (Fig. 3a), transporting warm air masses from the subtropical North Atlantic, mostly from the latitude belt of 25–40°N. Many of these trajectories also flow towards Northwestern Africa before entering the IP, as suggested by the high trajectory densities over that region (Fig. 3a). Despite the apparent advective nature of the WWE, in the latest stage the trajectories show clear stationarity (Fig. 3b and c) with important residence times over the inner IP. The corresponding streamlines reveal that a strong anticyclonic flow over Northwestern Africa plays a central role in generating these episodes, as they induce strong southwesterly winds over Iberia (Fig. 3a–c). The large median longitudinal displacement (approximately 60°) is much more pronounced than the corresponding meridional displacement (of only about 5°, Fig. 3d). This result highlights that these air parcels are transported by the prevailing westerly winds over the North Atlantic at nearly constant velocity, and then decelerated over the IP. The paths for the extremes in the five subsectors are clearly similar, suggesting similar driving mechanisms of WWE episodes for the entire IP. The peculiar northward displacement at the latest stage of the trajectories for N and CW suggest that the air parcels are first transported to inner Iberia, as is in fact illustrated by the high density over that region 1 d before onset (Fig. 3c).

The air parcel subsidence is relatively strong (250 hPa in 10 d, Fig. 3e), as well as the associated adiabatic warming (almost 30°C). Over the 10 d of the median trajectories, there is significant diabatic cooling of almost 10°C (Fig. 3f), which is, however, largely overcompensated by the aforementioned adiabatic warming through air parcel descent, eventually leading to a temperature increase of about 18°C (Fig. 3f). The median of the collocated 2-m maximum temperature remains nearly constant and is relatively high (around 15°C, Fig. 3g). Surface fluxes do not play a major role (Fig. 3h), except for the final stage of the trajectories, when they are nearly stationary over the IP at low-tropospheric levels. The strengthening of SLHF (enhanced evaporation) over Iberia is worth noting, as well as the enhanced fluxes of STR and SSR at the latest stage of the trajectories, indicating cloud-free conditions. For WWE episodes, there is a sharp increase in the specific humidity towards the latest stage of the trajectories, reaching median values as high as 6 g kg^{-1} at near-surface levels. However, owing to the relatively high temperatures during these episodes, the median of the relative humidity remains near 50% (Fig. 6b). This result also shows that the specific humidity increase is mostly compensated by air parcel warming.

Hence, the warm and cold winter extreme temperature episodes tend to arise due to totally different atmospheric flow regimes. While meridional transport plays a key role in triggering WCE episodes, zonal transport, followed by near stationarity over the IP, tends to favour WWE episodes. In both cases, adiabatic warming of the air parcels is predominant over the diabatic cooling along the trajectories, resulting in a net air parcel temperature increase of approximately 20°C in 10 d. Stronger adiabatic warming for WWE is accompanied by stronger diabatic cooling. Near-surface diabatic warming through surface fluxes is more noticeable for WCE episodes, definitively contributing to a significant moderation of these cold spells, which are indeed much less severe in the IP than over the rest of Europe. WCE episodes are also characterized by cold and very dry (continental) air masses, whilst WWE episodes are associated with relatively warm and more humid (maritime) air masses.

3.3. Summer cold extremes

SCE episodes are typically associated with northwesterly flow from the high-latitude North Atlantic (Fig. 4a–c). Unlike WCE episodes, the SCE trajectories are predominantly located over the ocean. Since the North Atlantic is colder than the IP in summer, cold extremes are naturally linked to maritime rather than continental pathways. Overall, synoptic-scale streamlines are in good agreement with trajectories, showing northwesterly winds towards Iberia (Fig. 4a–c), in response to cyclonic troughs over Western Europe and westward shifted Azores high-pressure systems. In fact, cold-core upper tropospheric troughs over Western/Northern Europe tend to be linked to these episodes (not shown), which is in agreement with the anomalously low near-surface temperatures during the SCE episodes. Both the meridional and zonal displacements of the trajectories are remarkable, roughly 20° and 40°, respectively (Fig. 4d), also reflecting the strong advective origin of these extremes. Additionally, their motion is at nearly constant speed along the entire trajectory.

Regarding the regional features, most trajectories come directly from the North Atlantic/Bay of Biscay, entering the IP through either the western coast (SW, CW and SE) or the northern coast (N and CE). A detailed analysis of the trajectory density patterns for each sector corroborates these results (not shown), but also highlights that an important number of trajectories for SE originate from the western Mediterranean. Two days before the SCE, the relatively cold air parcels surround the IP (Fig. 4b) and then gradually converge over the IP. This horizontal confluence of the air masses is driven by rising air motions over

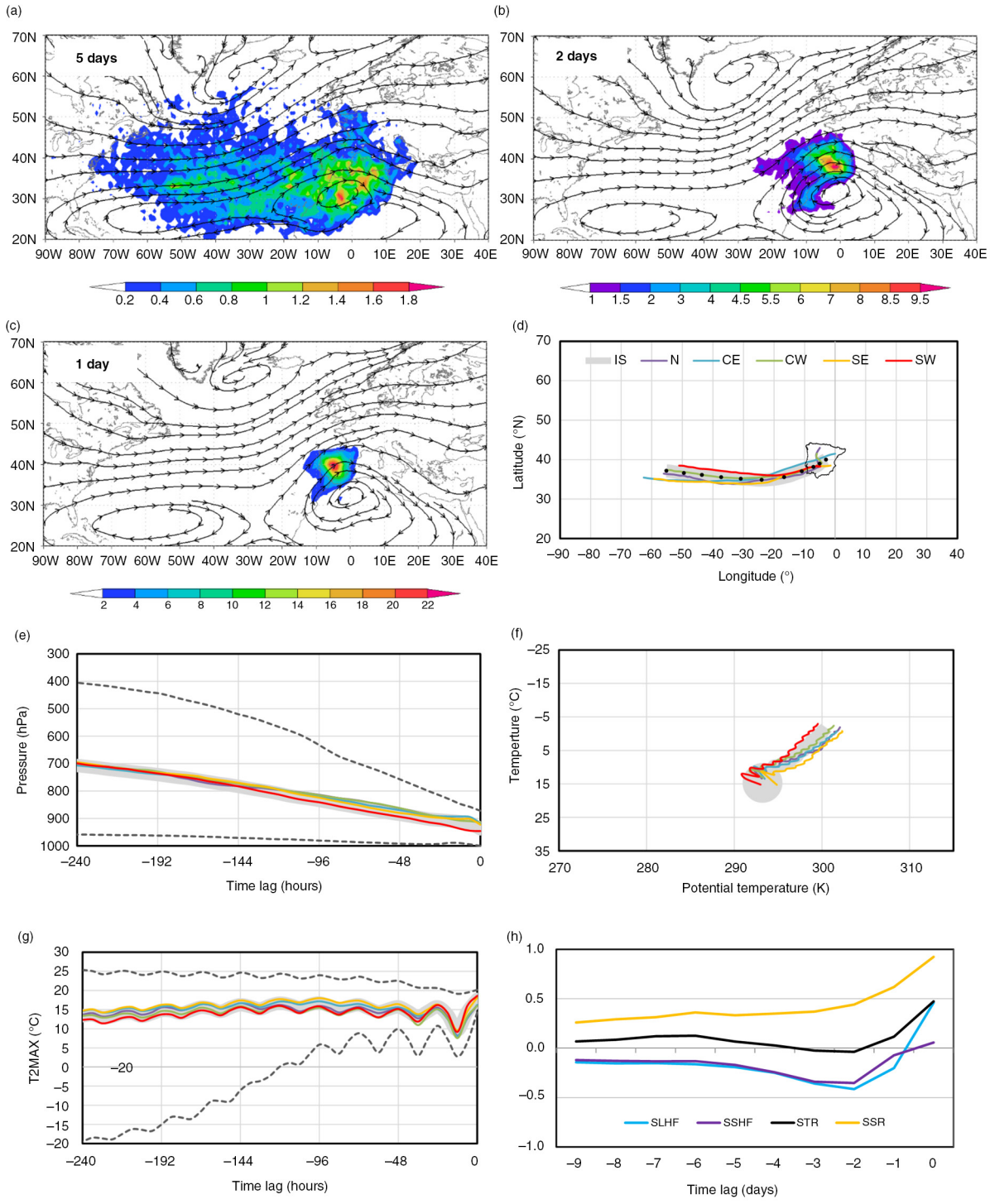

Fig. 3. As in Fig. 2, but for wintertime (DJF) extremely warm episodes, WWE.

the innermost parts of the peninsula. Further, the relatively high trajectory density over the western Mediterranean 1–2 d before the extreme event onset is mostly related to trajectories that recently entered the Mediterranean Basin from the North Atlantic over southern France (not shown).

The descent along the SCE trajectories is comparatively weak (100 hPa in 10 d), meaning that the adiabatic heating

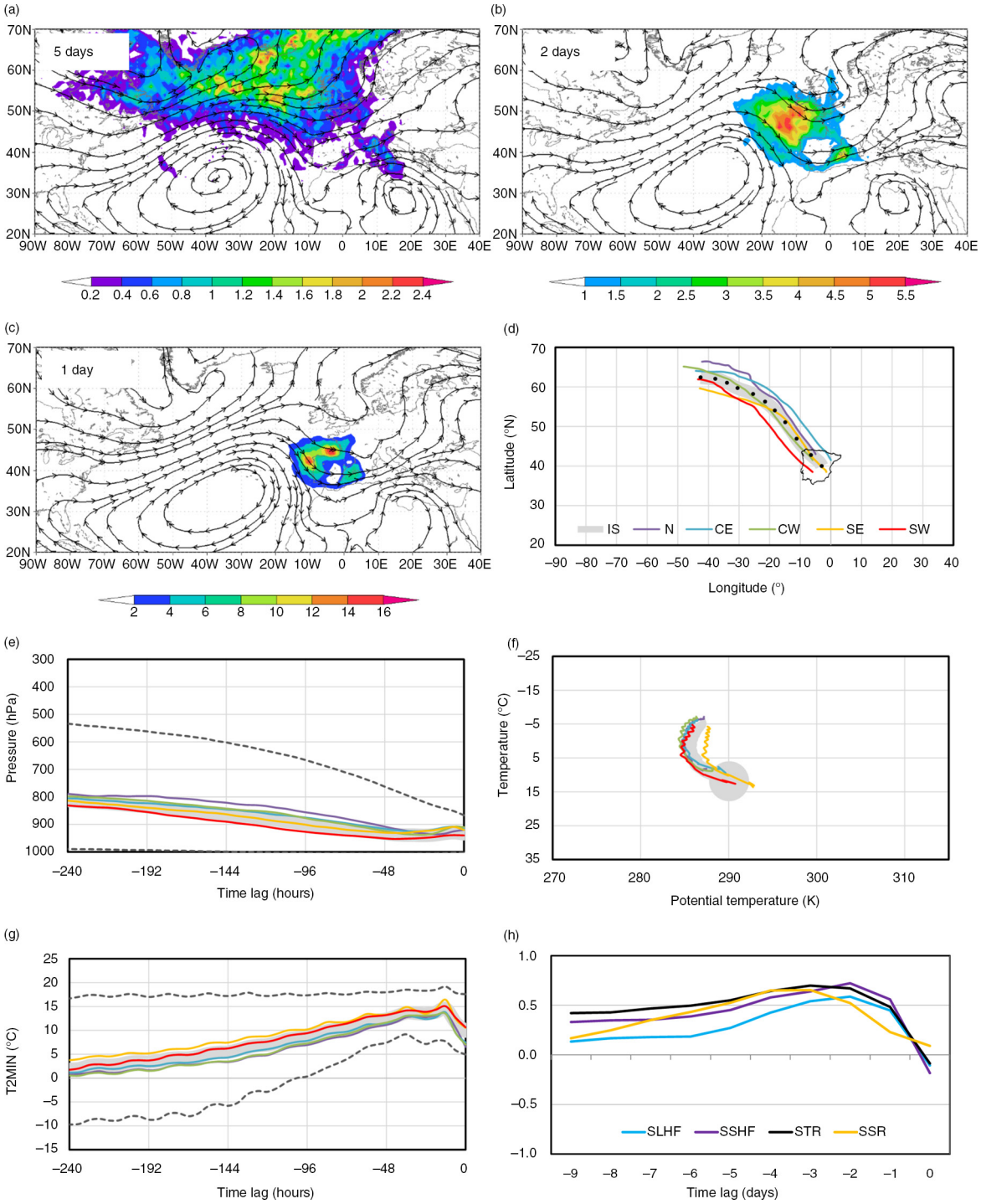

Fig. 4. As in Fig. 2, but for summertime (JJA) extremely cold episodes, SCE.

is also weak compared to the other categories (Fig. 4e), at most 15°C in 10 d. This fact also contributes to establishing the SCE episodes. The median air parcel temperature increases by about 15°C (Fig. 4f), which is due to the adiabatic warming enhanced by strong diabatic warming near the surface (Fig. 4f). The collocated 2-m minimum air temperature exhibits a steady increase, with median temperatures varying from nearly 2 to 15°C, but with a strong cooling at the latest stage of the trajectories, when the air mass is over land (Fig. 4g). This evolution reflects the southward displacement of the air parcels over the North Atlantic, as sea surface temperatures progressively increase,

emphasizing the key role of advection for the occurrence of SCE episodes. The nocturnal cooling over the IP at the latest stage of the trajectories also plays a role for the extremeness of the 2-m minimum temperature.

The aforementioned diabatic heating might be explained by important near-surface fluxes, which is clearly supported by positive anomalies in all fluxes (Fig. 4h), particularly from 5 to 1 d before SCE onset. Regarding the humidity parameters for the SCE episodes, the air parcel moistening is quite clear for the median trajectory, as it descends and approaches the surface, achieving a final (median) specific humidity of nearly 8 g kg^{-1}. Furthermore, relative humidity experiences a slow increase from 70% to 80%, followed by a steep decrease back to 70%. This behaviour is similar to the WCE episodes, but with slightly higher values (Fig. 6a and c). Air parcel moistening is widely compensated by warming, explaining the weak changes in relative humidity. On the whole, the maritime characteristics of air parcels are noticeable, suggesting relatively cold and wet weather conditions during SCE episodes in the IP.

3.4. Summer warm extremes

The SWE episodes tend to be associated with westerly and northwesterly flow from the North Atlantic at very early stages, but mainly with easterly/northeasterly flow in the later stages of the trajectories, followed by comparatively high residence times over or near the IP (Fig. 5a–c). The composite mean streamlines for these episodes demonstrate that anticyclonic circulation over Northwestern Africa generates southerly flow of continental tropical air masses towards the IP (Fig. 5a–c). However, results of the Lagrangian approach do not corroborate this synoptic perspective: the highest trajectory densities are in fact found over surrounding seas, and very low densities actually over Northern Africa. It should be kept in mind that streamlines do not correspond to actual air parcel trajectories in transient flow regimes, indicating the added value of the Lagrangian approach for analysing these episodes.

The near stationarity of the air masses over the IP 1–2 d before onset is clearly illustrated by the spiral trajectories for all subsectors (Fig. 5d). After moving 3–4 d at nearly constant speed towards Iberia, they remain stationary over the peninsula during the last 6–7 d before the episode onset. Further, most air masses associated with extreme heat over the IP approach the region from the north and not from the south. The high density of trajectories over the water surfaces surrounding the peninsula 1–2 d before SWE onset is the footprint of shallow low-pressure systems (heat lows) that induce convergence (spiralling) flows towards the inner peninsula, similarly to the SCE episodes. The connection between these mesoscale systems and temperature extremes in Iberia has been discussed, for example, in Pfahl (2014). The increased trajectory density to the east and northeast is also consistent with the occurrence of extremes over Iberia in association with atmospheric blocking events over Europe. While in many European regions warm temperature extremes occur in the vicinity of a blocking anticyclone (Pfahl and Wernli, 2012), for the IP the anticyclones are typically shifted to the north-east, which may lead to easterly/northeasterly transport of warm, continental air masses (Pfahl, 2014). Furthermore, there is no clear southerly inflow from North Africa, but rather easterly/southeasterly flow from the southern Mediterranean/Gibraltar Straight area towards the inner IP, strengthened by the wind channelling effect. This is particularly clear for SW and CW (not shown).

Moderate to strong air mass subsidence contributes to important adiabatic heating of the air masses associated with SWE episodes (Fig. 5e). The temperature of the air parcel increases by about 25°C (Fig. 5f), resulting from adiabatic warming in the first period (increased advective processes) and very strong and rapid diabatic warming during the 2 d before SWE onset (Fig. 5f). During this period of weak advection, the air masses acquire different thermodynamic characteristics, progressively warming, clearly expressed by the steep increase of the 2-m maximum temperature (Fig. 5g). Note also the increasing footprint of the diurnal cycle in the temperature evolution, as the trajectories enter the mixing layer (Fig. 5f). This behaviour is not surprising for 2-m maximum temperatures in summer. These results hint at strong surface diabatic heating during the last stage of the trajectories, also supported by the positive anomalies of STR and SSR (Fig. 5h).

The specific humidity evolution for SWE episodes is quite similar to that for SCE episodes (Fig. 6c and d), as in both cases the trajectories are of maritime origin and are gradually moistened as they descend into the boundary layer. Nevertheless, specific humidity is higher for SWE than for SCE at the earliest stages of the trajectories, due to the lower latitudes and warmer air masses involved (Figs. 4 and 5). Conversely, their relative humidity evolution is radically different (Fig. 6c and d). In fact, there is a remarkable decrease during the second half of the trajectory for the SWE episodes (last 5 d). This occurs in spite of the increase in specific humidity, stressing the strong warming during this final period.

Although the SCE and SWE episodes present fairly similar trajectory density patterns during the last days before the onset of the temperature extreme (a footprint of the Iberian summer heat low), the thermodynamic processes are fundamentally different. The origin of the trajectories is at much higher latitudes for SCE than for SWE, partially explaining the genesis of these episodes. Nonetheless, the much stronger adiabatic warming for SWE

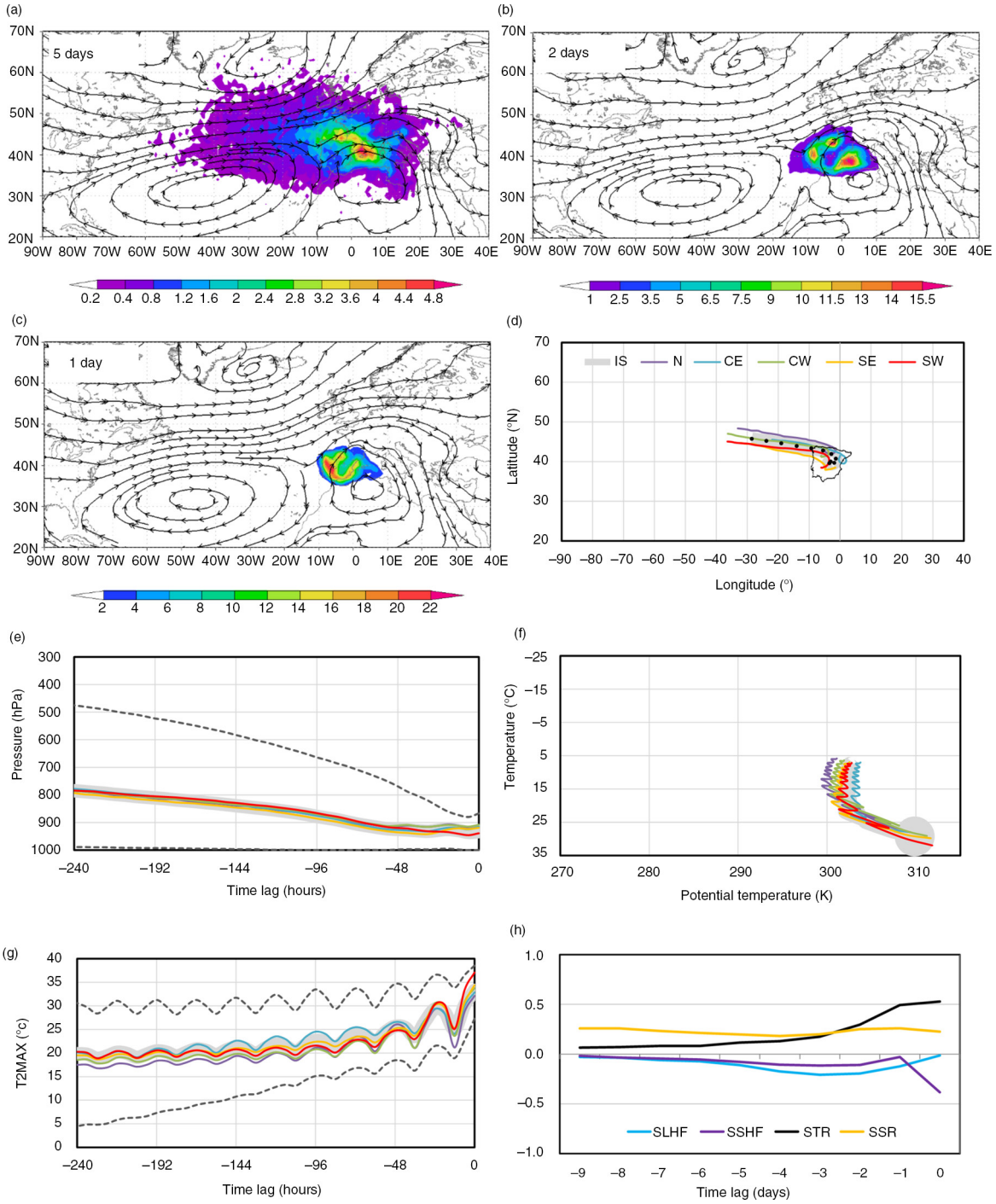

Fig. 5. As in Fig. 2, but for summertime (JJA) extremely warm episodes, SWE.

than for SCE clearly reinforces these differences in the air mass origins. Additionally, the longer residence times over the IP for SWE than for SCE yield much stronger diabatic warming by surface fluxes for SWE, enhancing the differences between these two contrasting categories. The SCE episodes are also associated with relatively cold and moist air masses, while the SWE episodes are characterized by very warm air masses, with high specific but low relative humidity.

3.5. *Temporal variability*

The occurrences of the extreme episodes are widely scattered over the entire period (1979–2012; Fig. 7), except for

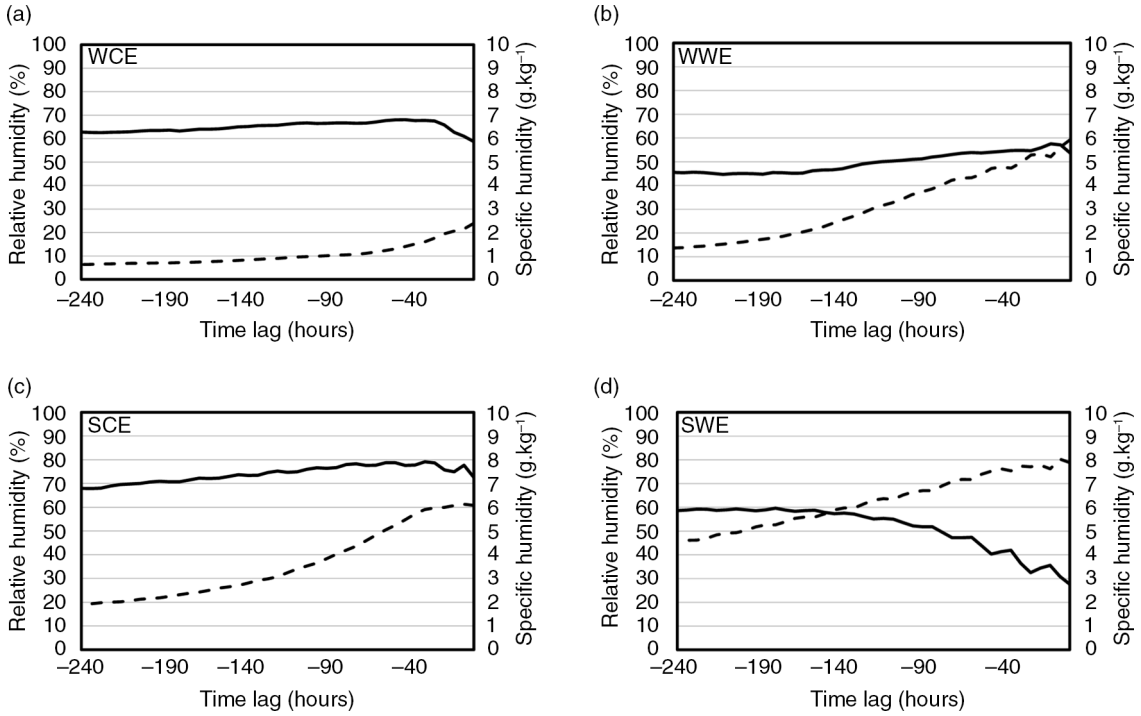

Fig. 6. Time series of the median of relative humidity (solid line) and specific humidity (dashed line) along the 10-d trajectories for each extreme episode: WCE, WWE, SCE and SWE for the entire Iberian sector.

SWE that shows a remarkable peak in summer 2003 (18% of all SWE occurrences). In fact, this summer, in particular August, was exceptionally warm, with a major heat wave and record-breaking temperatures over large areas of Europe (e.g. Schär et al., 2004; Garcia-Herrera et al., 2010), including the IP. According to ERA-Interim 2-m temperatures, SWE episodes were particularly frequent in the period of 1–13 August 2003, reaching a peak on 12 August, when nearly one third of the Iberian sector (cf. Section 2) recorded a SWE episode. The trajectory densities and corresponding streamline composites for all SWE episodes in summer 2003 display similar patterns to Fig. 5 (not shown), but with enhanced anticyclonic circulation over North Africa and the western-central Mediterranean, extending as a ridge towards northern France and diverting the westerly flow to northern Europe. Other summers with high daily SWE occurrences (not necessarily heat waves) were 1991 and 2012 (Fig. 7d). Relatively high daily occurrences are found during the winters of 1983, 1985, 1987, 2005 and 2012 for the WCE episodes (Fig. 7a), and in the winters of 1985, 1989, 1990, 1998 and 2000 for the WWE episodes (Fig. 7b). The SCE episodes were more frequent in the winters of 1984 and 1992 (Fig. 7c). Other extraordinary events include the 15 January 1985, when about 80% of the Iberian sector was under a WCE episode, and 6 June 1984, during which about 80% of the Iberian sector was under a SCE episode.

4. Summary and discussion

The present study explores the mechanisms underlying the occurrence of temperature extremes affecting the IP, using a Lagrangian investigation of the associated atmospheric flow. Only temperatures in the 1%-tails of the empirical distributions at each grid point are considered. Due to strong seasonality, winter and summer are analysed separately. Four temperature extremes are then selected: wintertime extremely cold and warm episodes (WCE and WWE, respectively) and summertime extremely cold and warm episodes (SCE and SWE). The WCE and SWE episodes correspond to the most extreme temperatures overall. The Lagrangian trajectories are isolated for each extreme and at each grid point in the IP domain, using the same methodology as in Bieli et al. (2014). For each episode type, their spatial densities (number of trajectories per km^2) are calculated over the North Atlantic–European sector up to 10 d before the episode onset. A complementary Eulerian description of the atmospheric flow is provided by the streamline composites of the 850 hPa wind fields for the temperature extreme days.

In winter, the WCE and WWE episodes are driven by clearly different atmospheric processes. Air parcel advection from the north governs the WCE episodes, whereas first eastward travelling air parcels that then become nearly stationary over the IP drive the WWE episodes. The 850 hPa

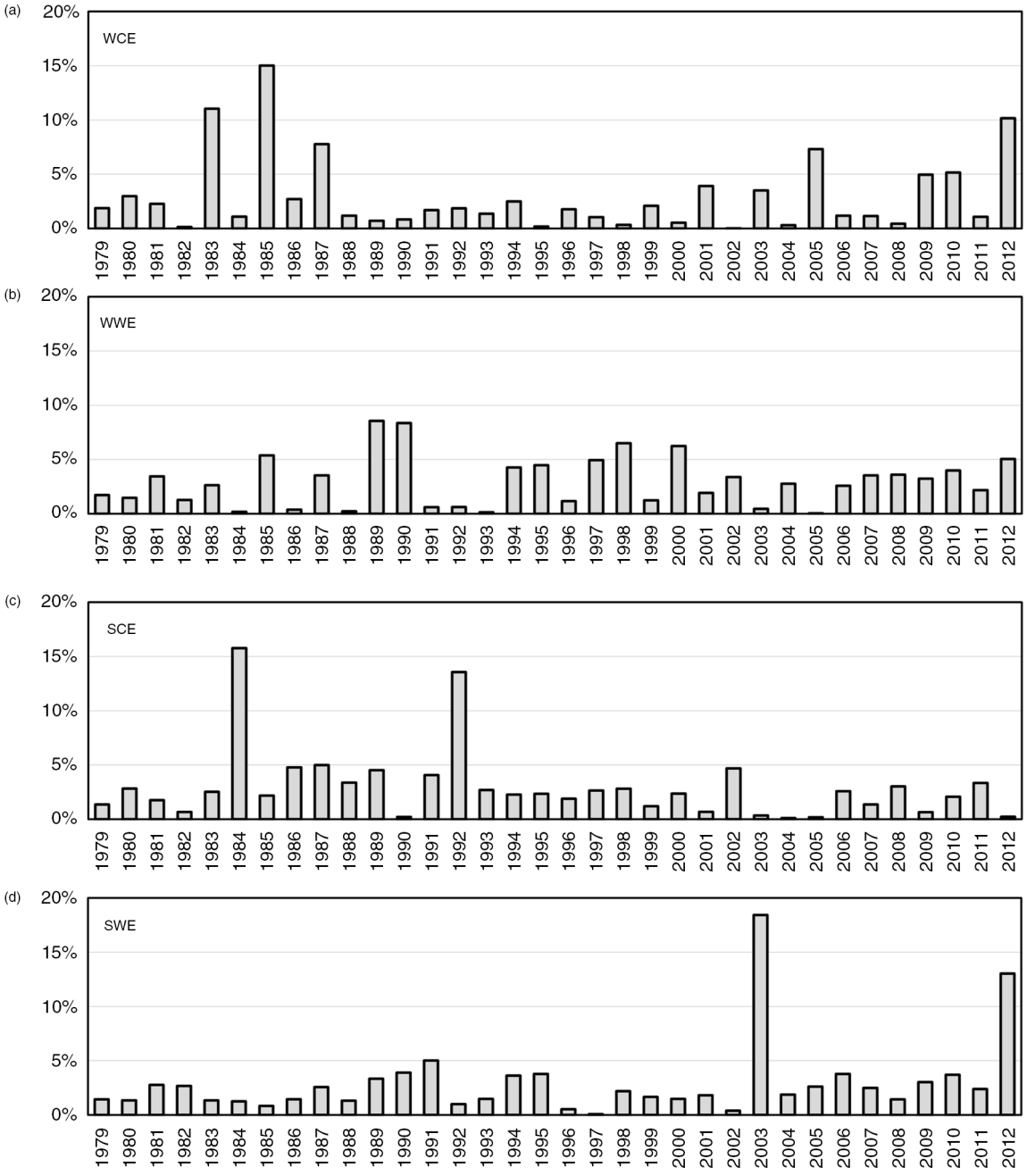

Fig. 7. Relative annual frequencies of occurrence (in%) of temperature extremes in the entire Iberian sector for: (a) WCE, (b) WWE, (c) SCE and (d) SWE.

streamlines for WCE hint at a quasi-stationary omega-like structure over the eastern North Atlantic that gradually strengthens, reaching its mature stage at the WCE onset, with an anticyclone over the British Isles and a cut-off low over Italy. These features suggest mid-latitude blocking over the eastern North Atlantic (e.g. Barriopedro et al., 2006), a negative phase of the EA pattern and anticyclonic Rossby wave-breaking over Europe (e.g. Woollings et al., 2008). The persistent southwestward transport to the IP driven by the blocking and downstream wave-breaking plays a key role in triggering these extremely cold episodes. Conversely, streamlines for the WWE episodes reveal strong southwesterly flow, due to a southwestward displaced Azores anticyclone and an anticyclonic circulation over North-western Africa. This pattern is clearly concomitant with the negative phase of the NAO (e.g. Hurrell et al., 2003).

For both extreme categories, adiabatic warming from air parcel descent tends to prevail over diabatic cooling along

the trajectories. For WWE, the stronger adiabatic warming is partially offset by stronger diabatic cooling. For both categories, the net air parcel warming is approximately 20°C in 10 d. For the WCE episodes, near-surface diabatic warming at the latest stage of the air parcel trajectories, mostly associated to SSHF and STR, considerably moderates the air mass extremeness. After the onset of the WCE, these processes further restore the extreme temperatures towards climatology. The humidity parameters suggest cold and dry continental air masses for WCE and warm and humid maritime air masses for WWE, which agrees with the respective trajectory paths.

For summer, both extreme episodes (SCE and SWE), particularly SWE, show clear footprints of the prevailing thermal low (low-tropospheric warm-core low-pressure system) over the IP. The heat low generates low-level wind jets along the coastal areas of the IP (Soares et al., 2014), which underlie the nearly circular shape of the trajectory densities. In contrast to winter, the association with teleconnection patterns, such as the NAO and EA, is less clear in summer, when the North Atlantic large-scale atmospheric circulation is generally much weaker (Barnston and Livezey, 1987). However, while for SCE episodes the Azores anticyclone is clearly separated from the anticyclonic circulation over North Africa, depicting a trough in between over the IP, for SWE episodes these two anticyclonic circulations are almost merged (Fig. 5a–c). As a result, northerly (southerly) flow prevails over the IP for SCE (SWE) episodes, with major implications in terms of the regional temperature. Furthermore, thermodynamic processes associated with SCE and SWE are quite different. First, trajectories originated at much higher latitudes for SCE than for SWE, which definitely contributes to the distinction between these two episodes. Second, there is a much stronger adiabatic warming for SWE (strong air parcel descent) than for SCE (weak descent). Third, the longer residence time of air parcels over land for SWE than for SCE significantly strengthens the near-surface diabatic warming, by surface fluxes and radiation, in the former. From the humidity parameters, it is shown that SCE episodes are characterized by cool maritime air masses, while the SWE episodes are characterized by very warm air masses with low relative humidity, despite the high moisture content. The results of the present study provide no evidence for trajectories coming from North Africa during SWE episodes, as suggested by the corresponding streamlines. In fact, their relatively high moisture content suggests maritime rather than continental origin, that is, high residence time over water surfaces surrounding the IP and not over North African dry land surfaces. These results also stress the significance of the Lagrangian description of the atmospheric flow for improving the current knowledge on temperature extremes.

The present study enabled a better understanding of the mechanisms underlying temperature extremes in Iberia from a large-scale perspective. The complex topography and resulting orographic effects in the IP, as well as the high land–sea thermal contrasts in summer, play an important role in the development of regional mesoscale systems. The poor resolution of these systems by ERA-Interim (ca. 80–100 km grid spacing) is an important limitation of the present study. Forthcoming studies could focus on a trajectory analysis on higher resolution grids (<10 km grid spacing), for example, as produced by Regional Climate Models (RCM) nested on ERA-Interim reanalysis (e.g. Soares et al., 2012) or on other higher resolution reanalysis datasets (Rienecker et al., 2011). Such a downscaling approach, which is very time consuming and beyond the scope of this first insight study, may enable more detailed path definitions and improve estimates of surface fluxes. They herein have shown to be critical for understanding the temperature extremes affecting the IP. Downscaling from global climate models may also be used to assess climate change signals on these mechanisms under future anthropogenic forcing (Kjellstrom et al., 2011), and thus also potentially contributing to a better risk management of climate extremes (Murray and Ebi, 2012) over Iberia.

5. Acknowledgements

This work is supported by national funds by FCT – Portuguese Foundation for Science and Technology, under the project PEst-OE/AGR/UI4033/2014. MeteoSwiss is acknowledged for providing access to ECMWF analysis data. We also would like to thank the anonymous reviewers for their valuable comments.

References

AEMET/IMP. 2011. *Iberian Climate Atlas*. Closas-Orcoyen S. L., Madrid, Spain.

Alexander, L. V., Zhang, X., Peterson, T. C., Caesar, J., Gleason, B. and co-authors. 2006. Global observed changes in daily climate extremes of temperature and precipitation. *J. Geophys. Res.* **111**, D05109. DOI: 10.1029/2005JD006290.

Andrade, C., Fraga, H. and Santos, J. A. 2014. Climate change multi-model projections for temperature extremes in Portugal. *Atmos. Sci. Lett.* **15**, 149–156.

Andrade, C., Leite, S. M. and Santos, J. A. 2012. Temperature extremes in Europe: overview of their driving atmospheric patterns. *Nat. Hazard. Earth Sys.* **12**, 1671–1691.

Barnston, A. G. and Livezey, R. E. 1987. Classification, seasonality and persistence of low-frequency atmospheric circulation patterns. *Mon. Weather Rev.* **115**, 1083–1126.

Barriopedro, D., Garcia-Herrera, R., Lupo, A. R. and Hernandez, E. 2006. A climatology of northern hemisphere blocking. *J. Clim.* **19**, 1042–1063.

Bieli, M., Pfahl, S. and Wernli, H. 2014. A Lagrangian investigation of hot and cold temperature extremes in Europe. *Q. J. Roy. Meteorol. Soc.* **141**, 98–108. DOI: 10.1002/qj.2339.

Cattiaux, J., Yiou, P. and Vautard, R. 2012. Dynamics of future seasonal temperature trends and extremes in Europe: a multi-model analysis from CMIP3. *Clim. Dynam.* **38**, 1949–1964.

Cony, M., Hernández, E. and Del Teso, T. 2008. Influence of synoptic scale in the generation of extreme cold days in Europe. *Atmosfera*. **21**, 389–401.

Cooney, C. M. 2012. Managing the risks of extreme weather: IPCC Special Report. *Environ. Health Perspect.* **120**, a58.

Decker, M., Brunke, M. A., Wang, Z., Sakaguchi, K., Zeng, X. B. and co-authors. 2012. Evaluation of the reanalysis products from GSFC, NCEP, and ECMWF using flux tower observations. *J. Clim.* **25**, 1916–1944.

Dee, D. P., Uppala, S. M., Simmons, A. J., Berrisford, P., Poli, P. and co-authors. 2011. The ERA-Interim reanalysis: configuration and performance of the data assimilation system. *Q. J. Roy. Meteorol. Soc.* **137**, 553–597.

Efthymiadis, D., Goodess, C. M. and Jones, P. D. 2011. Trends in Mediterranean gridded temperature extremes and large-scale circulation influences. *Nat. Hazard. Earth Sys.* **11**, 2199–2214.

Field, C. B., Barros, V., Stocker, T. F., Qin, D., Dokken, D. J. and co-authors. 2012. *Managing the Risks of Extreme Events and Disasters to Advance Climate Change Adaptation: Summary for Policymakers*. A Special Report of Working Groups I and II of the Intergovernmental Panel on Climate Change. Cambridge University Press, Cambridge, UK.

Fischer, E. M. and Schär, C. 2010. Consistent geographical patterns of changes in high-impact European heatwaves. *Nat. Geosci.* **3**, 398–403.

Frías, M., Mínguez, R., Gutiérrez, J. and Méndez, F. 2012. Future regional projections of extreme temperatures in Europe: a nonstationary seasonal approach. *Clim. Change*. **113**, 371–392.

Garcia-Herrera, R., Diaz, J., Trigo, R. M., Luterbacher, J. and Fischer, E. M. 2010. A review of the European summer heat wave of 2003. *Crit. Rev. Environ. Sci. Tecnol.* **40**, 267–306.

García-Herrera, R., Hernández, E., Barriopedro, D., Paredes, D., Trigo, R. M. and co-authors. 2007. The outstanding 2004/05 drought in the Iberian Peninsula: associated atmospheric circulation. *J. Hydrometeorol.* **8**, 483–498.

Hanson, C., Palutikof, J., Livermore, M., Barring, L., Bindi, M. and co-authors. 2007. Modelling the impact of climate extremes: an overview of the MICE project. *Clim. Change*. **81**, 163–177.

Holton, J. R. 2004. *An Introduction to Dynamic Meteorology*. Elsevier, London, UK.

Hurrell, J. W., Kushnir, Y., Ottersen, G. and Visbeck, M. 2003. An overview of the North Atlantic Oscillation. In: *The North Atlantic Oscillation: Climatic Significance and Environmental Impact* (eds. J. W. Hurrell, Y. Kushnir, G. Ottersen and M. Visbeck). American Geophysical Union, Washington, DC, USA, pp. 1–35.

IPCC. 2013. Climate change 2013: the physical science basis. In: *Contribution of Working Group I to the Fifth Assessment Report of the Intergovernmental Panel on Climate Change* (eds. T. F. Stocker, D. Qin, G.-K. Plattner, M. Tignor, S. K. Allen and co-editors). Cambridge University Press, Cambridge, UK, 1535 pp.

Kharin, V. V., Zwiers, F. W., Zhang, X. and Wehner, M. 2013. Changes in temperature and precipitation extremes in the CMIP5 ensemble. *Clim. Change*. **119**, 345–357.

Kjellstrom, E., Nikulin, G., Hansson, U., Strandberg, G. and Ullerstig, A. 2011. 21st century changes in the European climate: uncertainties derived from an ensemble of regional climate model simulations. *Tellus A*. **63**, 24–40.

Mahlstein, I., Martius, O., Chevalier, C. and Ginsbourger, D. 2012. Changes in the odds of extreme events in the Atlantic basin depending on the position of the extratropical jet. *Geophys. Res. Lett.* **39**, L22805. DOI: 10.1029/2012GL053993.

Moore, G. W. K. and Renfrew, I. A. 2012. Cold European winters: interplay between the NAO and the East Atlantic mode. *Atmos. Sci. Lett.* **13**, 1–8.

Murray, V. and Ebi, K. L. 2012. IPCC special report on managing the risks of extreme events and disasters to advance climate change adaptation (SREX). *J. Epidemiol. Community Health.* **66**, 759–760.

Orlowsky, B. and Seneviratne, S. I. 2012. Global changes in extreme events: regional and seasonal dimension. *Clim. Change*. **110**, 669–696.

Pfahl, S. 2014. Characterising the relationship between weather extremes in Europe and synoptic circulation features. *Nat. Hazards Earth Syst. Sci.* **14**, 1461–1475.

Pfahl, S. and Wernli, H. 2012. Quantifying the relevance of atmospheric blocking for co-located temperature extremes in the Northern Hemisphere on (sub-)daily time scales. *Geophys. Res. Lett.* **39**, L12807. DOI: 10.1029/2012GL052261.

Ramos, A., Trigo, R. and Santo, F. 2011. Evolution of extreme temperatures over Portugal: recent changes and future scenarios. *Clim. Res.* **48**, 177–192.

Rienecker, M. M., Suarez, M. J., Gelaro, R., Todling, R., Bacmeister, J. and co-authors. 2011. MERRA: NASA's modern-era retrospective analysis for research and applications. *J. Clim.* **24**, 3624–3648.

Santos, J. and Corte-Real, J. 2006. Temperature extremes in Europe and wintertime large-scale atmospheric circulation: HadCM3 future scenarios. *Clim. Res.* **31**, 3–18.

Santos, J. A., Corte-Real, J., Ulbrich, U. and Palutikof, J. 2007. European winter precipitation extremes and large-scale circulation: a coupled model and its scenarios. *Theor. Appl. Climatol.* **87**, 85–102.

Santos, J. A., Reis, M. A., De Pablo, F., Rivas-Soriano, L. and Leite, S. M. 2013a. Forcing factors of cloud-to-ground lightning over Iberia: regional-scale assessments. *Nat. Hazard. Earth Sys.* **13**, 1745–1758.

Santos, J. A., Woollings, T. and Pinto, J. G. 2013b. Are the winters 2010 and 2012 archetypes exhibiting extreme opposite behavior of the North Atlantic jet stream? *Mon. Weather Rev.* **141**, 3626–3640.

Schär, C., Vidale, P. L., Lüthi, D., Frei, C., Häberli, C. and co-authors. 2004. The role of increasing temperature variability in European summer heatwaves. *Nature*. **427**, 332–336.

Seneviratne, S. I., Donat, M. G., Mueller, B. and Alexander, L. V. 2014. No pause in the increase of hot temperature extremes. *Nat. Clim. Change*. **4**, 161–163.

Seneviratne, S. I., Nicholls, N., Easterling, D., Goodess, C. M., Kanae, S. and co-authors. 2012. Changes in climate extremes and their impacts on the natural physical environment. In: *Managing the*

Risks of Extreme Events and Disasters to Advance Climate Change Adaptation (eds. C. B. Field, V. Barros, T. F. Stocker, D. Qin, D. J. Dokken and co-editors), Cambridge University Press, Cambridge, UK, pp. 109–230.

Sillmann, J., Croci-Maspoli, M., Kallache, M. and Katz, R. W. 2011. Extreme cold winter temperatures in Europe under the influence of North Atlantic atmospheric blocking. *J. Clim.* **24**, 5899–5913.

Soares, P. M., Cardoso, R., Miranda, P. A., Medeiros, J., Belo-Pereira, M. and co-authors. 2012. WRF high resolution dynamical downscaling of ERA-Interim for Portugal. *Clim. Dynam.* **39**, 2497–2522.

Soares, P. M. M., Cardoso, R. M., Semedo, Á., Chinita, M. J. and Ranjha, R. 2014. Climatology of the Iberia coastal low-level wind jet: weather research forecasting model high-resolution results. *Tellus A*. **66**, 22377, DOI: http://dx.doi.org/10.3402/tellusa.v66.22377

Solomon, A., Goddard, L., Kumar, A., Carton, J., Deser, C. and co-authors. 2011. Distinguishing the roles of natural and anthropogenically forced decadal climate variability implications for prediction. *B Am Meteorol Soc*. **92**, 141–156.

Tank, K. A. M. G. and Können, G. P. 2003. Trends in indices of daily temperature and precipitation extremes in Europe, 1946–99. *J. Clim.* **16**, 3665–3680.

Trigo, R. M., Osborn, T. J. and Corte-Real, J. M. 2002. The North Atlantic Oscillation influence on Europe: climate impacts and associated physical mechanisms. *Clim. Res.* **20**, 9–17.

Trigo, R. M., Pozo-Vazquez, D., Osborn, T. J., Castro-Diez, Y., Gamiz-Fortis, S. and co-authors. 2004. North Atlantic oscillation influence on precipitation, river flow and water resources in the Iberian peninsula. *Int. J. Climatol.* **24**, 925–944.

Tullot, I. F. 2000. *Climatologia de Espana y Portugal*. Ediciones Universidad de Salamanca, Salamanca.

Ulbrich, U., Christoph, M., Pinto, J. G. and Corte-Real, J. 1999. Dependence of winter precipitation over Portugal on NAO and baroclinic wave activity. *Int. J. Climatol.* **19**, 379–390.

Walsh, J. E., Phillips, A. S., Portis, D. H. and Chapman, W. L. 2001. Extreme cold outbreaks in the United States and Europe, 1948–99. *J. Clim.* **14**, 2642–2658.

Wernli, H. and Davies, H. C. 1997. A Lagrangian-based analysis of extratropical cyclones. I: the method and some applications. *Q. J. Roy. Meteorol. Soc.* **123**, 467–489.

Woollings, T., Hannachi, A. and Hoskins, B. 2010. Variability of the North Atlantic eddy-driven jet stream. *Q. J. Roy. Meteorol. Soc.* **136**, 856–868.

Woollings, T., Hoskins, B., Blackburn, M. and Berrisford, P. 2008. A new Rossby wave-breaking interpretation of the North Atlantic Oscillation. *J. Atmos. Sci.* **65**, 609–626.

Zhang, X., Alexander, L., Hegerl, G. C., Jones, P., Tank, A. K. and co-authors. 2011. Indices for monitoring changes in extremes based on daily temperature and precipitation data. *WIRES Clim. Change*. **2**, 851–870.